Microstructure and wear behaviour of Ni-based alloy coated onto grey cast iron using a multi-step induction cladding process

Jing Yu[a],*, Bo Song[a], Yanchuan Liu[b]

[a] Marine Engineering College, Dalian Maritime University, Dalian 116026, China
[b] Dalian Special Equipment Inspection Institute, Dalian 116013, China

ABSTRACT

The purpose of this work was to develop an innovative approach to remanufacturing grey cast iron cylinder liners. Ni-based alloy coatings were fabricated on HT 300 cast iron substrates using a multi-step induction cladding technique. Scanning Electron Microscopy (SEM), Energy Dispersive X-ray Spectroscopy (EDS) and X-ray Diffraction (XRD) were employed to analyse the microstructure, elemental distribution and phase composition of the coating. The results indicated that the coatings were metallurgically bonded to the substrate, and there were no visible defects and cracks at the interface resulting in failure of the coating. The portion closest to the substrate was rich in γ-Ni solid solution, whereas the intermediate and top portions consisted of boride-, carbide- and Ni-based solid solution eutectics. The microhardness from the top layer of the coating to the interface exhibited a gradual decrease, and the average microhardness of the coating is $877.12\,HV_{0.2}$, which was four times higher than that of the substrate. The results of dry sliding wear tests showed that the friction coefficient of the Ni-based alloy coating was much more consistent than that of the HT 300 substrate, and the wear loss and roughness of the coating was lower than that of the substrate. The wear mechanism for the coating is light abrasive wear, whereas for the substrate, the wear mechanism is a mixture of severe abrasive and adhesive wear.

Due to its good machinability, castability, thermal conductivity, shock absorption, self-lubrication, and low price, grey cast irons [1] are widely used in cylinder liners for medium- and large-scale marine diesel engines [2]. In recent years, increasing technical requirements for diesel engines, such as higher combustion pressures and operating temperatures to achieve higher power and lower fuel consumption, have accelerated the wear and cavitation of cylinder liners. Therefore, it is crucial to remanufacture used cylinder liners to enhance the utilization ratio of marine machinery components. To remanufacturing cylinder liners either in service or retired, surface technology can be applied to recover the original dimensions and performance [3], including electroplating, thermal spraying, welding, laser cladding and induction cladding. Among them, the coatings deposited by electroplating and thermal spraying are mechanical bonding to the substrate, and therefore the thickness of coating is limited; in contrast, the coatings fabricated by welding, laser cladding and induction cladding have dense microstructure and are metallurgical bonding to the substrate.

Induction cladding is an emerging environmentally friendly surface cladding technology that combines the advantages of induction heating and surface coating technologies [4]. This technique can fabricate coatings with high resistances to wear and corrosion and has the advantage of being used in many previous studies to prepare Ni-based and Fe-based alloy coatings on steel substrates. Chang et al. fabricated a Ni-based alloy coating on a steel substrate using vacuum induction melting and analysed the influence of the sliding distance and velocity on the wear mechanism under dry sliding conditions [5]. Hu et al. studied the microstructure and wear resistance of a Ni-based alloy coating on a medium carbon steel substrate. The results showed that the main wear mechanism for the coating was mild adhesive wear, whereas the dominant wear mechanism for the substrate was severe abrasive wear [6]. Grey cast irons, common materials for cylinder liners, contain a large amount of graphite and have poor weldability, commonly resulting in cracks at the interface between the cladding layer and the substrate [7]. Furthermore, the melting point of grey cast iron is low and close to that of the alloy powder, making it difficult to the control processing parameters during induction cladding. Therefore, it is vital to extensively discuss fabricating alloy coating on the grey cast iron using induction cladding. However, depositing alloy coatings on grey cast irons has rarely been investigated [8].

In this study, Ni-based alloy coatings were fabricated on HT 300 cast

---

Table 1
Chemical compositions (wt.%) of the substrate and coating alloy.

Content/wt.%	Element						
	C	Cr	B	Si	Mn	Ni	Fe
HT 300	2.5–4.0	–	–	1.0–2.5	0.5–1.4	–	Bal.
SH-Ni 60A	0.6–1.0	15–20	3.0–4.5	4.0–5.5	–	Bal.	≤5

Table 2
Optimal parameters for the induction cladding process.

	Plan A			Plan B
	Preheating	Heating 1	Heating 2	Heating
Current/A	10	20	30	10
Heating Time/s	90	90	11	303
Frequency/kHz		32–36		

iron substrates using a multi-step induction cladding method. The microstructure, phase composition, and elemental distribution of the coating and interface were analysed. To evaluate the wear resistance, ball-on-disc experiments without lubrication were carried out at room temperature. The findings from this study are expected to provide an innovative approach for remanufacturing cylinder liners.

Experimental procedure

Materials

The materials used here were HT 300 cast iron as the substrate and a Ni-based alloy powder (SH-Ni 60A) to prepare the induction cladding coating. The Ni-based alloy powder is composed of spherical particles with diameters in the range from 45 to 106 µm. The chemical compositions of these metals are listed in Table 1. Cylindrical specimens were machined with a diameter of 22 mm and height of 100 mm. To clean, roughen, and activate the surface of the substrate, grit blasting was used, followed by ultrasonic cleaning in an alcohol solution before drying in hot air. The Ni-based alloy powder was mixed with a supersaturated solution of sodium silicate and then deposited on the substrate using a 3D printed mould to form a pre-coated layer with a thickness of 1 mm, as shown in Fig. 1(a). The substrate with a pre-coated layer was dried at 200 °C for 3 h and then directly placed inside a graphite crucible for induction cladding.

Induction cladding process

The induction cladding experimental system was composed of a induction cladding equipment (maximum current of 150 A; maximum frequency of 40 kHz), a rotary platform, a helical heating coil, cooling, and temperature monitoring systems, as shown in Fig. 1(b). The temperature was measured using two non-contact infrared pyrometers,

which could measure temperatures in ranges from 250 to 2000 °C and 500 to 2500 °C at the surface and substrate, respectively. During the cladding process, the Ni-based alloy layer was heated to 1254 °C until it was red and glowing. After performing numerous initial experiments, we determined that an optimized multi-step heating process with varying power increments (Plan A) or with low and constant power heating for a long period (Plan B) resulted in the highest quality coatings, as listed in Table 2. However, for prolonged heating times, a large quantity of heat is conducted to the substrate, resulting in significant heat damage. Considering this, the optimal cladding process parameters are described in Plan A.

Characterization of the Ni-based alloy coating

Metallographic samples were cut along the radial direction of the induction cladding specimens and subsequently mounted in an epoxy resin. The surface was polished with #200 to #1500 emery papers, buffed to a mirror finish, and polished using 1 µm diamond powder. The samples were etched with a mixture of 50 ml hydrochloric acid, 50 ml distilled water, and 5 g cupric sulphate. The morphology and microstructure of the transverse section were observed using SEM (SUPRA 55 SAPPHIRE, ZEISS International, Germany). The elemental distribution at the interface between the coating and substrate was determined using EDS coupled to the SEM. The phase composition of the coating was identified using XRD (EMPYEAN, PANalytical B.V., the Netherlands).

The transverse cross-section microhardness of the coating from the layer surface to the substrate was measured using a semi-automatic Vickers microhardness tester (LW-HV 1000, Beijing Leweiwulian Science and Technology Co., Ltd., China) with a 200 g load and a dwell time of 20 s. The distance between each measured point was 50 µm, and each microhardness value was derived from three measurement points.
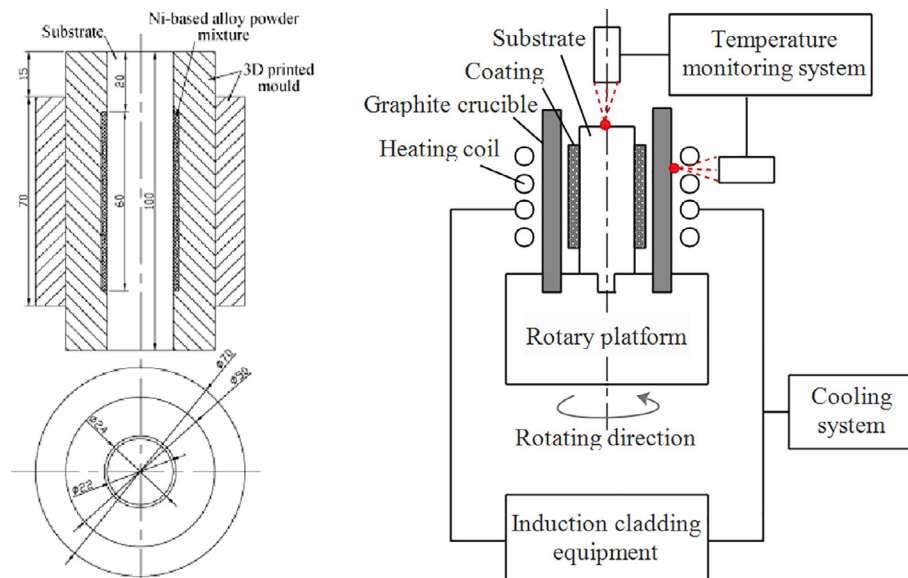

Fig. 1. Schematic illustration of (a) the coating deposition mould and (b) the experimental system.

The error quoted here was the standard error in the mean.

Dry sliding wear test

Wear tests were performed on a ball-on-disc wear tester (CFT-I, Lanzhou Zhongkekaihua Science and Technology Co., Ltd., China) at room temperature without lubrication. A tungsten carbide ball with a diameter of 4 mm and hardness of 1400 $HV_{0.2}$ was utilized as a counterball. The wear tests were conducted on the surface of the Ni-based alloy coating and HT 300 substrate, respectively, with the wear parameters being a constant load of 20 N, a fixed reciprocating distance of 5 mm, frequency of 10 Hz, and a fixed sliding time of 3000 s. The Ni-based coating and HT 300 substrate were cut into specimens by a wire cutting machine with an area of 10×10 mm and then mounted in epoxy resin with a diameter of 30 mm and height of 10 mm to meet the requirements for the testing shape. Prior to testing, the wear surfaces were polished and buffed. The morphologies of the wear surface were observed by SEM, and the 3D topography, average cross-sectional area of wear scars and roughness of the worn surface were detected by a three-dimensional confocal microscope (LEXT OLS 300, OLYMPUS, Japan). To decrease the experimental data fluctuation, three repeated wear tests were conducted, and an average value was presented.

Results and discussion

Microstructure

Fig. 2(a) shows the morphology of the cross-section of the Ni-based alloy coating on the HT 300 substrate. A clear boundary was observed between the coating and the substrate, with a high-quality interface and no visible defects or cracks (such features can result in flaking of the coating). Moreover, several pores were observed within the coating, which are commonly generated by two different mechanisms: (1) gaps between the solid alloy powders particles that cannot be filled by the melted powder during the processing time and (2) the diffusion rate of residual gas in the coating being lower than the solidification rate, resulting in the gas being trapped and forming pores. The bottom of the cladding layer (closest to the substrate) was composed of a Ni-based solid solution and clusters of tiny graphite flakes, as shown in Fig. 2(b). Hu et al. called this region the transition zone and proposed that it indicates metallurgical bonding between the coating and substrate [6].

During induction cladding, intense eddy currents at the interface induce a high temperature at the bottom of cladding layer [9]. As the substrate is at a low temperature, a temperature gradient G occurs around the interface region. In addition, the bottom layer of the coating remains molten for a long period, decreasing the solidification rate R, and resulting in relatively large G/R values. Ni atoms act as the crystal nuclei for the solid solution. The crystals absorb Ni atoms from the nearby molten cladding layer and grow accordingly. Therefore, a concentration of Ni occurs at the bottom of the coating near the interface, resulting in the primary phase composition being γ-Ni in this region. With increasing distance from the interface, the G/R decreases rapidly, resulting in dendrites forming in the cladding layer. The Ni- based alloy powder used here contained high amounts of Cr, C, and B. Owing to the high amount of Ni confined at the interfacial region, there was a concentration gradient of Ni between the bottom of the molten pool and the top, whereas the Cr, C, and B gradually diffused and migrated into the intermediate layer. As a result, we observed some boride-, carbide- and Ni-based eutectics dispersed in the middle and top regions of the coating, as shown in Fig. 2(c). Such a microstructure was similar to that observed in materials produced by direct laser cladding [10] and the high velocity oxygen fuel (HVOF) spraying samples with a post-treatment NiCrBSi coating [11]. Obvious layer phenomenon can be observed in the cross-section of the coating, which has fine planar crystallization, a zone with eutectic morphology and heterogeneous precipitates distributed in the metallic matrix successively from the interface to the top
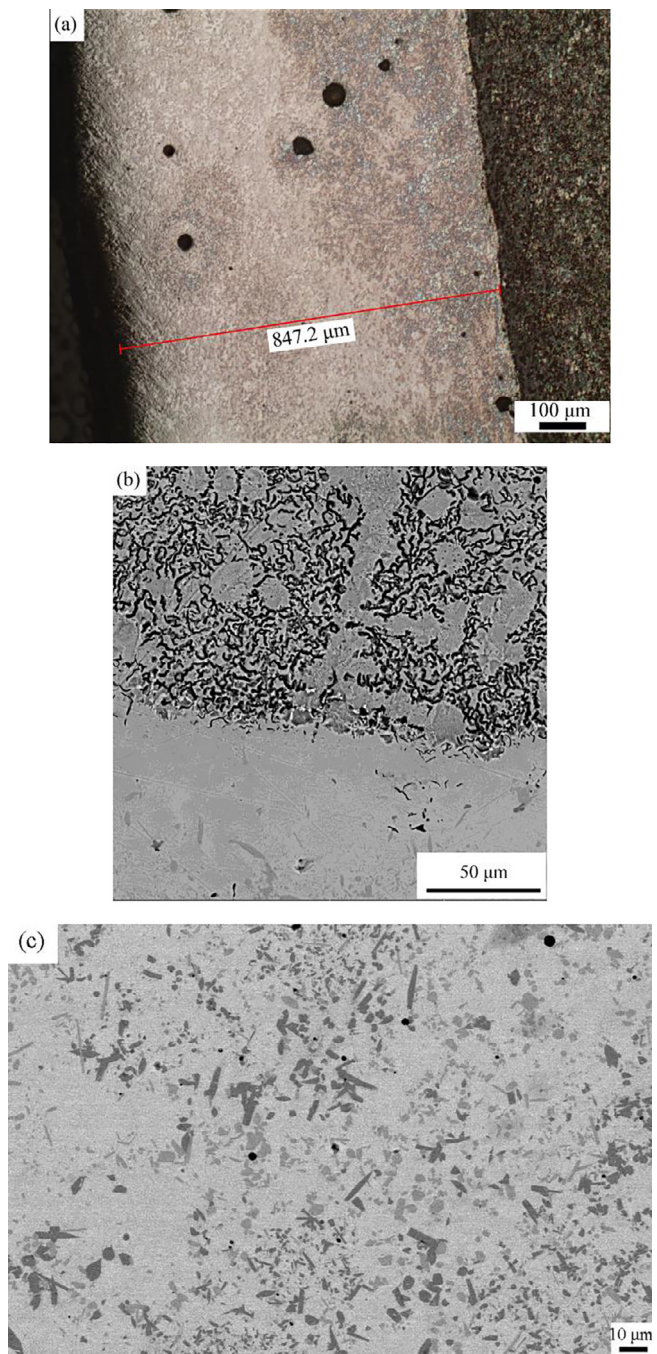

Fig. 2. Morphology and microstructure of the substrate coated with Ni-based alloy coatings (a) the morphology of the coating, (b) the interface between the coating and substrate, and (c) the intermediate coating.

layer of the coating.

Elemental diffusion and phase analysis

The elemental distribution at the interface is shown in Fig. 3. The obvious interdiffusion of elements demonstrates the metallurgical bonding between the coating and the substrate. At the interface, Fe from the substrate clearly diffused into the coating, whereas a smaller quantity of Ni and Cr in the coating diffused into the substrate. This phenomenon can be explained as follows. During the induction cladding process, the fusible alloy in the coating melts first, whereas only a very narrow layer of the surface of the substrate melts (or no melting occurs). Therefore, it is easier for Fe from the substrate to diffuse into
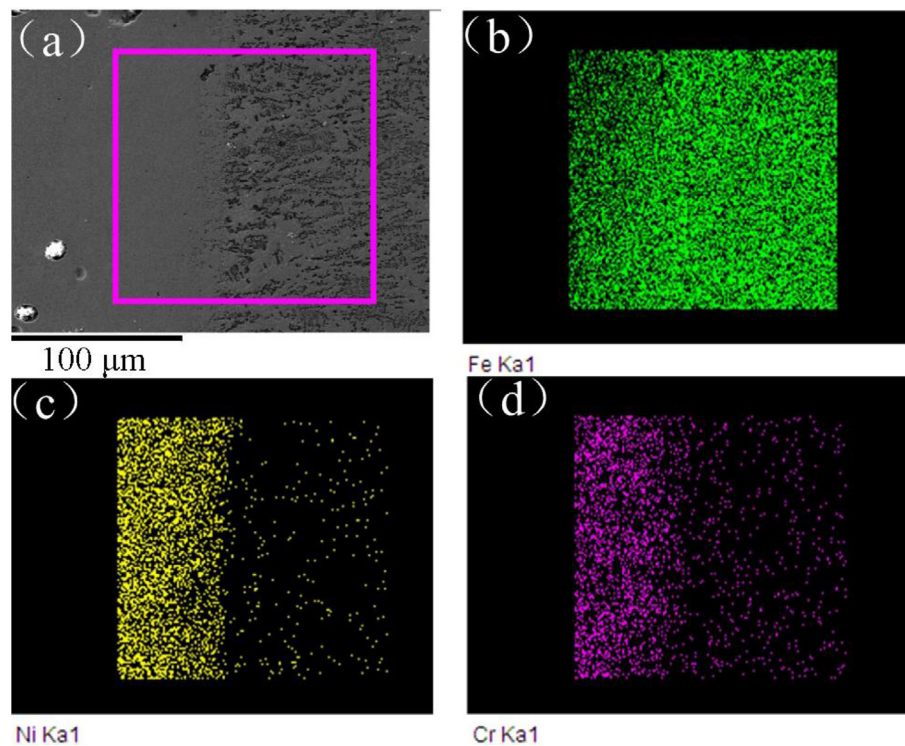
Fig. 3. Elemental distribution at the interface: (a) SEM image showing the location of EDS surface scan distributions of (b) iron, (c) chromium, and (d) nickel.

the molten coating, and it is more difficult for elements in the coating to diffuse into the solid substrate.

The XRD pattern for a representative coating is shown in Fig. 4. The phase composition of the coating was complex and included γ-Ni, Ni_3Si, $Cr_{1.12}Ni_{2.88}$, Ni_3B, and $Cr_{15.58}Fe_{7.42}C_6$. The main phase observed in the coating was dendritic γ-Ni solid solution. In addition, there were dispersed compounds containing dissolved Si and Cr, along with some hard phases, such as Ni_3B and $Cr_{15.58}Fe_{7.42}C_6$. The precipitation of borides and carbides in the coating is beneficial for increasing the hardness and resistance to abrasive and adhesive wear [5,6].

Microhardness

Fig. 5 shows the variation in the microhardness profile over the transverse cross-section of the Ni-based alloy coating on the HT 300 substrate. It reveals that an intergradation in the microhardness appeared at the interface between the coating and substrate, which helps to improve the adhesion of the coating to substrate [12]. In addition, the morphology of measured indentation also indicated the changing trend in the microhardness from the coating to the substrate. The average hardness of the coating was approximately 877.12 $HV_{0.2}$ and that of the substrate was 220.48 $HV_{0.2}$. The hardness of the coating was four times higher than that of the substrate because the top layer of molten coating rapidly solidified during induction cladding, resulting in
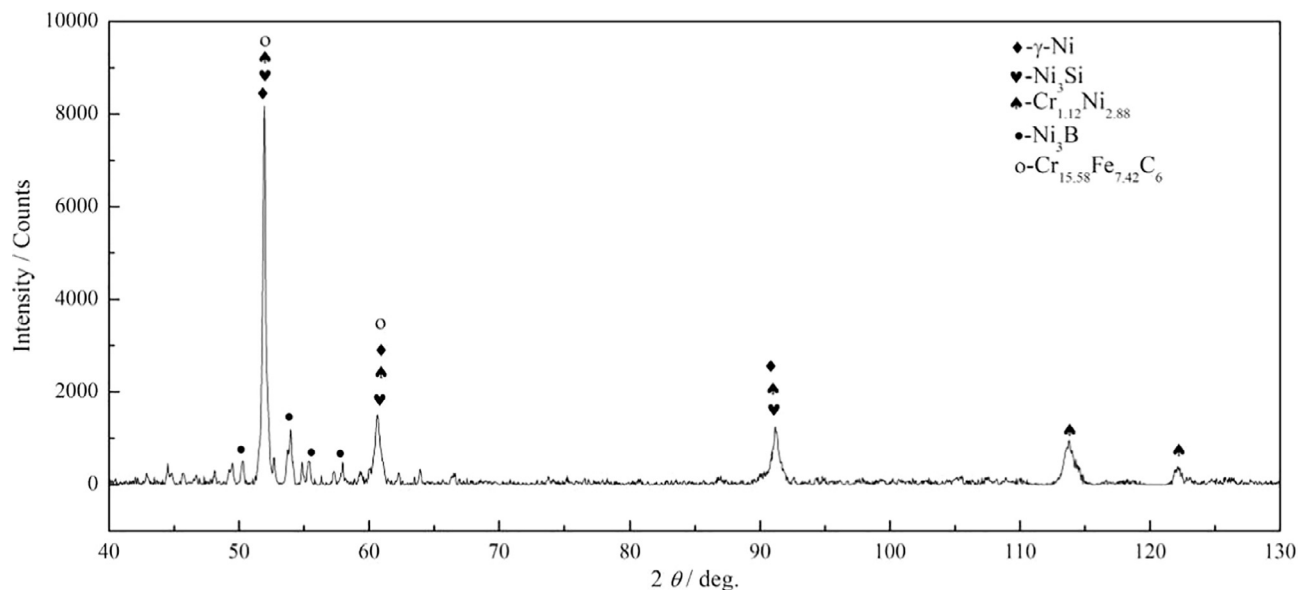

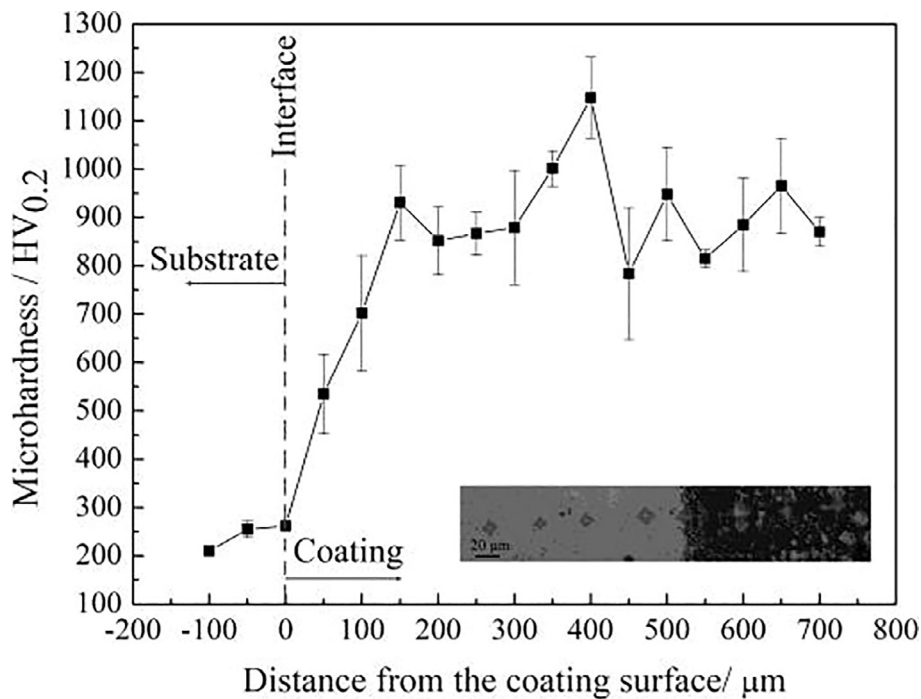**Fig. 4.** X-ray diffraction spectrum of the Ni-based coating.

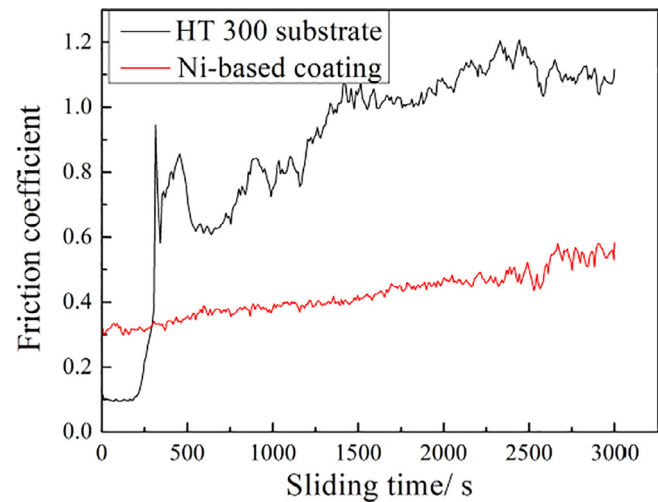Fig. 5. Microhardness profile in the transverse cross-section of the Ni-based coating.

Fig. 6. Friction coefficients for the Ni-based coating and substrate under dry sliding wear conditions.

Table 3
Wear test results from the coating and substrate under dry sliding wear conditions.

Material	Average cross-sectional area/mm^2	Wear volume/mm^3	Average surface roughness/µm
Ni-based coating	2.073	1.037	2.210
HT 300 substrate	25.497	12.749	5.056

fine grain strengthening. Moreover, large amounts of hard borides Ni$_3$B and carbides Cr$_{15.58}$Fe$_{7.42}$C$_6$ were uniformly scattered in the intermediate and top layer of coating. The decrease in microhardness at the interface was ascribed to the extremely high heat transfer rate between the molten alloy coating and the substrate, leading to the interdiffusion of iron and fine lamellar graphite from the substrate to the coating, which resulted in the chemical composition in the coating being diluted by elements in the substrate. Furthermore, the heat transfer was slow at the interface, which resulted in the bottom layer being primarily composed of the soft phases γ-Ni and Ni$_3$Si.
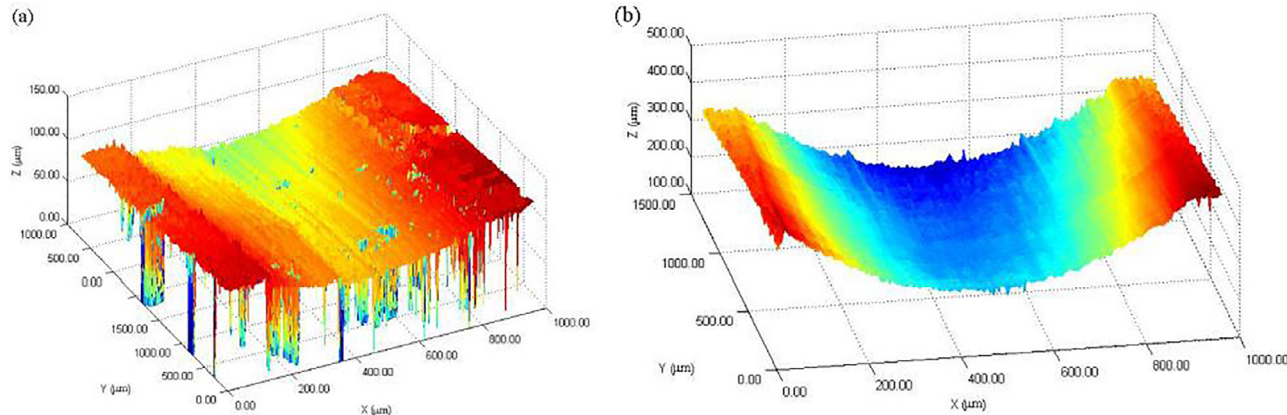

Fig. 7. 3D topographies of wear tracks for the (a) coating and (b) substrate.
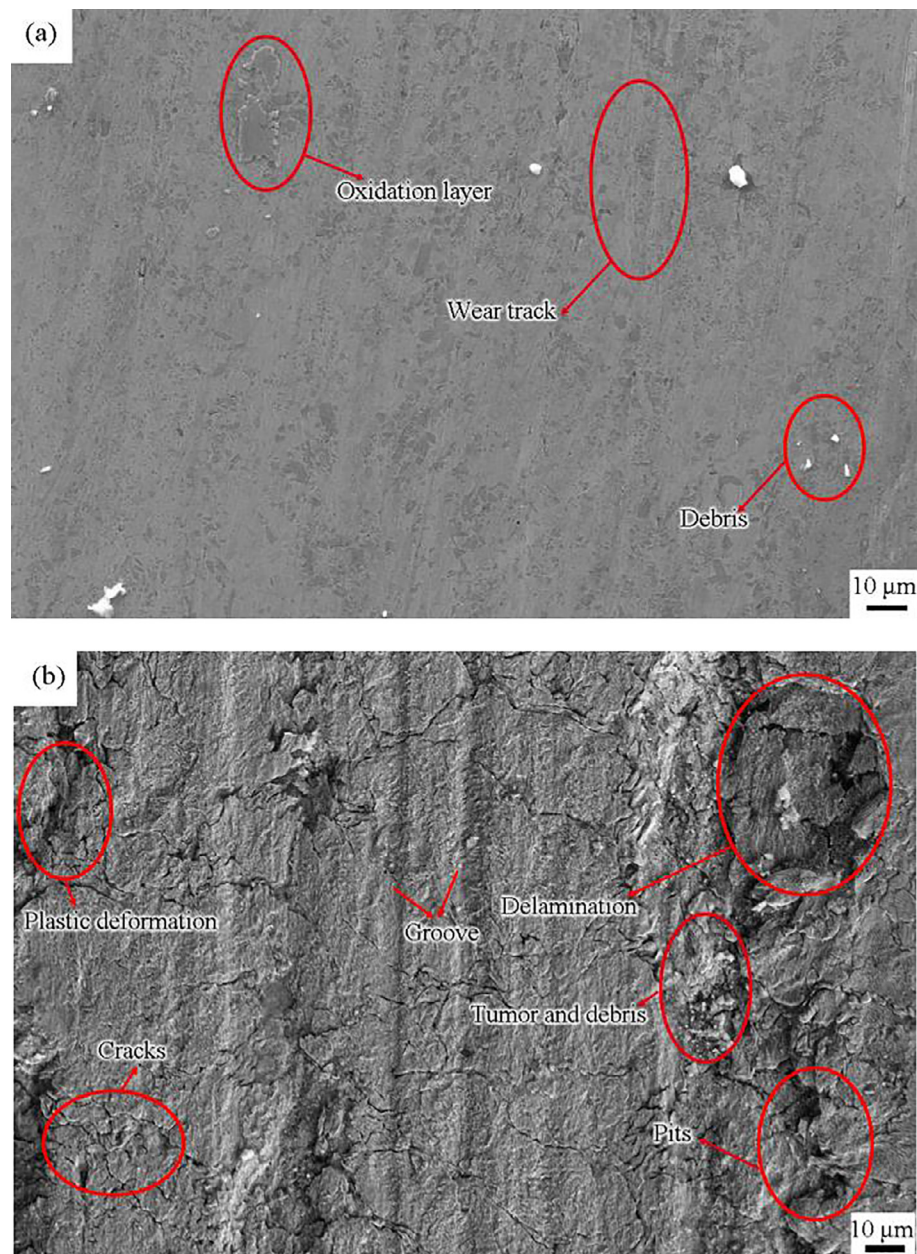
Fig. 8. Morphologies of the worn surfaces of the (a) Ni-based coating and (b) HT 300 substrate under dry sliding conditions.

Wear resistance and behaviour

Fig. 6 shows the friction coefficients of the Ni-based alloy coating and HT 300 substrate as a function of sliding time. The friction coefficients of both the coating and substrate increase with the sliding time. The friction coefficient for the coating changes slightly and the ranges from 0.30 to 0.58. The friction coefficient of the substrate fluctuates violently and ranges from 0.58 to 1.21. According to the Archard theory [13], the hardness of metal materials is proportional to the wear resistance, whereas it is inversely proportional to the friction coefficient. Therefore, it can be concluded that the stability of the wear resistance of the coating was better than that of the substrate.

Wear track 3D topographies for the coating and substrate are shown in Fig. 7. The average cross-sectional area of the coating was lower than that of the substrate, and consequently, the wear volume of the coating was less than that of the substrate. The average surface roughness of the coating was lower than that of the substrate, as shown in Table 3. It can be concluded that the wear resistance of the substrate can be improved significantly by using the coating.

Fig. 8(a) shows the morphologies of worn surfaces for the Ni-based alloy coating under dry sliding conditions. A minor quantity of small white particles was observed. Light scratches were present in the soft phase γ-Ni solid solution and Ni_3Si. Chang et al. affirmed that the debris remained on the worn surface of the Ni-based coating was NiO using EDS and XRD [5]. The scraped-up metal was oxidized due to the heat generated from wear process, forming oxide particles, some of which remained at the worn surface. Owing to the hard phases Ni_3B and $Cr_{15.58}Fe_{7.42}C_6$ being dispersed in the coating, the hardness of the coating was improved significantly, notably enhancing its ability to withstand plastic deformation and its adhesive wear resistance. In addition, a dense oxidation layer was attached to the worn surface. The presence of the oxidation layer was caused primarily by the debris remained at the surface being compressed by the loading. The formation of the oxidation layer was beneficial for preventing the original surface from experiencing any direct wear [5]. In conclusion, the dry sliding wear mechanism for the Ni-based alloy coating is light abrasive wear.

Sever wear occurred at the worn surface of the HT 300 substrate under dry sliding conditions, as shown in Fig. 8(b), including the presence of ploughing grooves parallel to the sliding direction, debris attachment to the worn surface, flake delamination, pitting, plastic deformation and cracking. During the wear process, the debris promoted three-body abrasive wear, and an increase in the amount of debris, tumours in some areas and a large amount of debris accumulating nearby. Owing to the much lower hardness of the substrate compared with the tungsten carbide counterball, it was easy for the hard surface of the counterball to penetrate into the contact surface of the substrate, resulting in the formation of grooves and plastic deformation. In addition, due to the repeated loading associated with sliding, fatigue cracks were observed at the worn surface. After a certain number of cycles, large flakes and blocked debris peeled off, resulting in some pits being generated at the worn surface. Therefore, the dominant dry sliding wear mechanism for the HT 300 substrate at room temperature is severe abrasive and adhesive wear.

Conclusions

To improve the reliability and durability of cylinder liners for marine diesel engines, Ni-based alloy coatings were fabricated on HT 300 cast iron substrates using a multi-step induction cladding technique. The conclusions from this work are as follows:

(1) The coating was metallurgically bonded to the substrate, and there were no visible defects or cracks at the interface (which can promote failure of the coating).
(2) The bottom part of the coating near the interface consisted of primarily a γ-Ni solid solution, and the intermediate and top layers contained large amounts of boride, carbide, and carbide + γ-Ni solid solution eutectics.
(3) The microhardness profile from the top layer of the coating to the interface displayed a gradual decrease. The average hardnesses of the coating and interface are four times and two times higher than

that of the substrate, respectively.
(4) Under dry sliding wear conditions, the friction coefficient of the Ni-based alloy coating was much more consistent than that of the HT 300 substrate, and the wear loss and roughness of the coating were lower than that of the substrate. The wear mechanism of the coating is slight abrasive wear, whereas that of the substrate is severe abrasive and adhesive wear. The wear resistance of the HT 300 grey cast iron substrate was improved significantly by using the induction cladding Ni-based alloy coating.

Acknowledgements

References

[1] Shen L, Li C. Wear 1991;147:195–206.
[2] Wiborg T, Eriksson J, Tjernaes A. Norw Marit Res 1974;2:2–11.
[3] Chang Y, Zhou D, Wang YL, Huang HH. J Mater Eng Perform 2016;25:5343–51.
[4] Chang JH, Liu TH, Chou JM, Hsieh RI, Lee JL. Mater Chem Phys 2010;120:702–8.
[5] Chang JH, Tzeng SK, Chou JM, Hsieh RI, Lee JL. Wear 2011;270:294–301.
[6] Hu G, Meng H, Liu J, Met T. Sci Heat Treat 2014;35:193–7.
[7] Arias-Gonzalez F, Del Val J, Comesana R, Penide J, Lusquinos F, Quintero F, et al. J Pou Appl Surf Sci 2016;374:197–205.
[8] Yu J, Song B. Mater Sci Forum 2017;909:33–8.
[9] Zhang Z, Han G, Fu Y, Shen L. J Mater Eng 2003:3–6.
[10] Navas C, Colaco R, de Damborenea J, Vilar R. Surf Coat Technol 2006;200:6854–62.
[11] Houdkova A, Smazalova E, Vostrak M, Schubert J. Surf Coat Technol 2014;253:14–26.
[12] Kim J, Xavier F, Kim D. Mater Des 2015;84:231–7.
[13] Archard JF. Surface topography and tribology. Tribology 1974;7(5):213–20.